Available online at www.sciencedirect.com
ScienceDirect
Trans. Nonferrous Met. Soc. China 35(2025) 3203−3217
Transactions of Nonferrous Metals Society of China
www.tnmsc.cn

Heterogeneous lamellar structure dominated mechanical properties optimization in ARBed Al alloy laminated metal composites

Tai-qian MO[1,2], Hua-qiang XIAO[2], Cun-hong YIN[2], Bo LIN[2], Xue-jian WANG[2], Kai MA[3]

1. Key Laboratory of Advanced Manufacturing Technology, Ministry of Education, Guizhou University, Guiyang 550025, China;
2. School of Mechanical Engineering, Guizhou University, Guiyang 550025, China;
3. Shi-changxu Innovation Center for Advanced Materials, Institute of Metal Research, Chinese Academy of Science, Shenyang 110016, China

Received 22 February 2024; accepted 26 August 2024

Abstract: 1060/7050 Al/Al laminated metal composites (LMCs) with heterogeneous lamellar structures were prepared by accumulative roll bonding (ARB), cold rolling and subsequent annealing treatment. The strengthening mechanism was investigated by microstructural characterization, mechanical property tests and in-situ fracture morphology observations. The results show that microstructural differences between the constituent layers are present in the Al/Al LMCs after various numbers of ARB cycles. Compared with rolled 2560-layered Al/Al LMCs with 37.5% and 50.0% rolling reductions, those with 62.5% rolling reductions allow for more effective improvements in the mechanical properties after annealing treatment due to their relatively high mechanical incompatibility across the interface. During tensile deformation, with the increased magnitude of incompatibility in the 2560-layered Al/Al LMC with a heterogeneous lamellar structure, the densities of the geometrically necessary dislocations (GNDs) increase to accommodate the relatively large strain gradient, resulting in considerable back stress strengthening and improved mechanical properties.

Key words: Al/Al laminated metal composites; heterogeneous lamellar structure; geometrically necessary dislocations (GNDs); back stress strengthening

1 Introduction

Laminated metal composites (LMCs) are prepared by metallurgically combining two or more metals with different performance characteristics; these materials can integrate the advantageous properties of constituent metals and possess certain superior characteristics that are difficult to achieve with a single material, such as good impact toughness and corrosion resistance [1,2]. In numerous LMC investigations to date, scholars have comprehensively examined the changes in microstructures after fabrication, with an emphasis on the impact of processing parameters on the mechanical properties [3,4]. However, the strengthening effect during the fabrication process is extremely limited, and one can expect that the mechanical properties of LMCs can be optimized via post-treatment, such as annealing [5] and thermomechanical treatment [6]. Moreover, the introduction of interfaces in LMCs increases the diversity of strengthening methods relative to traditional metals. In addition, exploring potential performance characteristics of materials based on their structural advantages is highly important.

Corresponding author: Bo LIN, Tel: +86-15285049061, E-mail: linbo1234@126.com
https://doi.org/10.1016/S1003-6326(25)66876-2

Furthermore, in-depth research on the interlayer and internal microscale strengthening mechanisms is beneficial for the development of high-performance metals and the improvement of their service capabilities in complex environments.

For the structural characteristics of layered materials, mechanical behaviors are usually defined by their interfacial attributes, such as the formation of a diffusion layer [7] and the occurrence of plastic instability [1,8]. Moreover, layer interfaces act as barriers against dislocation motion, significantly contributing to strengthening; in addition, decreased interfacial space can improve the mechanical properties [9]. Furthermore, multiple interfaces during plastic deformation can effectively increase the fracture toughness of LMCs, which is attributed mainly to crack arrest and deflection phenomena [10].

Another strategy for improving the mechanical properties of LMCs is to regulate the micro-structures between the constituent layers to construct a reinforced structure. Many reinforced structures, such as gradient structures [11], heterogeneous lamellar structures [12,13] and bimodal structures [14], have been investigated to solve the inversion problem of strength and ductility. Among these reinforced structures, heterogeneous lamellar structures have been developed to potentially achieve high strength and ductility in metals due to the microscopic strengthening effect introduced by the incompatible deformation between microstructures [13]. The accumulation of geometrically necessary dislocations (GNDs) near the interface of the soft layer in the heterogeneous lamellar structure during plastic deformation leads to the formation of strain gradients, promoting additional strain hardening and back stress strengthening. Related research has been extensively conducted on stainless steels [15], titanium alloys [16], and copper alloys [17]. However, most of the existing methods for tailoring heterogeneous structures are focused on the dynamic recrystallization and solid-state phase transition of single metals. Although many researchers have focused on multiscale interface strengthening based on differences in the structures of dissimilar metals in LMCs [9,18], reports on the strengthening mechanisms of heterogeneous lamellar structures in LMCs are rare, and identifying their formation method is also challenging.

In this investigation, Al/Al LMCs containing AA1060 and AA7050 were used as a bimetal system and were processed by accumulative roll bonding (ARB) and subsequent cold rolling. The effects of annealing post-treatment on the microstructural and mechanical properties of multilayered Al/Al LMCs were explored, with an emphasis on the impacts of heterogeneous lamellar structures. The aim of this study was to further optimize the mechanical properties and service capacities of LMCs by introducing reinforced structures, providing a new perspective for the structural design of laminated metal composites with excellent performance.

2 Experimental

2.1 Material preparation

Commercial pure aluminum AA1060 and high-strength aluminum alloy AA7050 were used as the raw materials for fabricating multilayered Al/Al LMCs with initial thicknesses of 1.5 mm and 2 mm, respectively. The chemical compositions of the two materials are provided in Table 1. The raw microstructures of AA1060 and AA7050, which were characterized by electron backscattered diffraction (EBSD), are shown in Fig. 1. As presented in Fig. 1(a), substantial equiaxed grains were detected, revealing a completely recrystallized structure in AA1060. In contrast, the initial microstructure of AA7050 mainly consisted of elongated grains, as shown in Fig. 1(b). In addition, according to the orientation distribution function (Figs. 1(c, d)), the strong cube (001)⟨100⟩ component of AA1060 and Goss (110)⟨001⟩ component of AA7050, which are typical recrystallization textures and rolling textures, were consistent with the microstructural features.

The preparation process of Al/Al LMCs was divided into two steps (Fig. 2): (1) ARB process: First, after surface treatment of the initial sheets, three layers of 1060 sheets and two layers of 7050 sheets were sequentially stacked into five-layered composite sheets and riveted for fixation. After holding at 400 °C for 10 min, the 8.5 mm stacked sheet was hot roll-bonded in one pass to 4 mm to obtain a 5-layered Al/Al LMC. Then, the roll-bonded composite was cut in half, and after surface treatment, the previous process was repeated for

Table 1 Chemical compositions of AA1060 and AA7050 alloys (wt.%)

Alloy	Zn	Mg	Cu	Si	Fe	Mn	Zr	Ti	Al
AA1060	0.05	0.03	0.05	0.25	0.35	0.03	–	0.03	Bal.
AA7050	6.20	2.20	2.20	0.10	0.10	–	0.13	–	Bal.

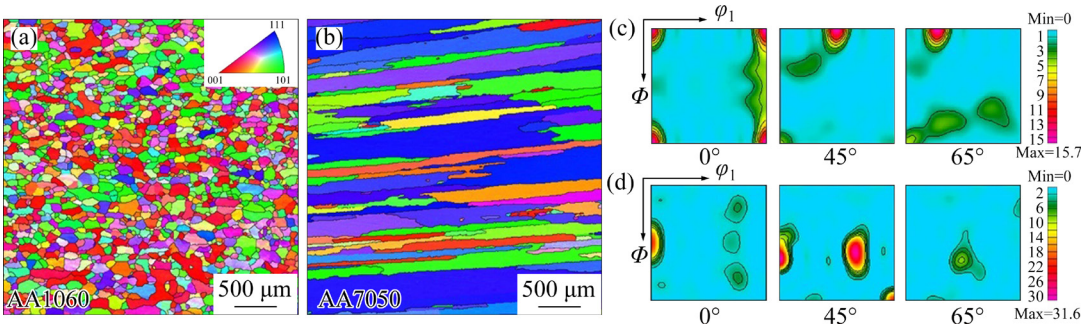

Fig. 1 IPF maps showing cross sections (a, b) and corresponding texture distributions (c, d) of AA1060 (a, c) and AA7050 (b, d) raw materials

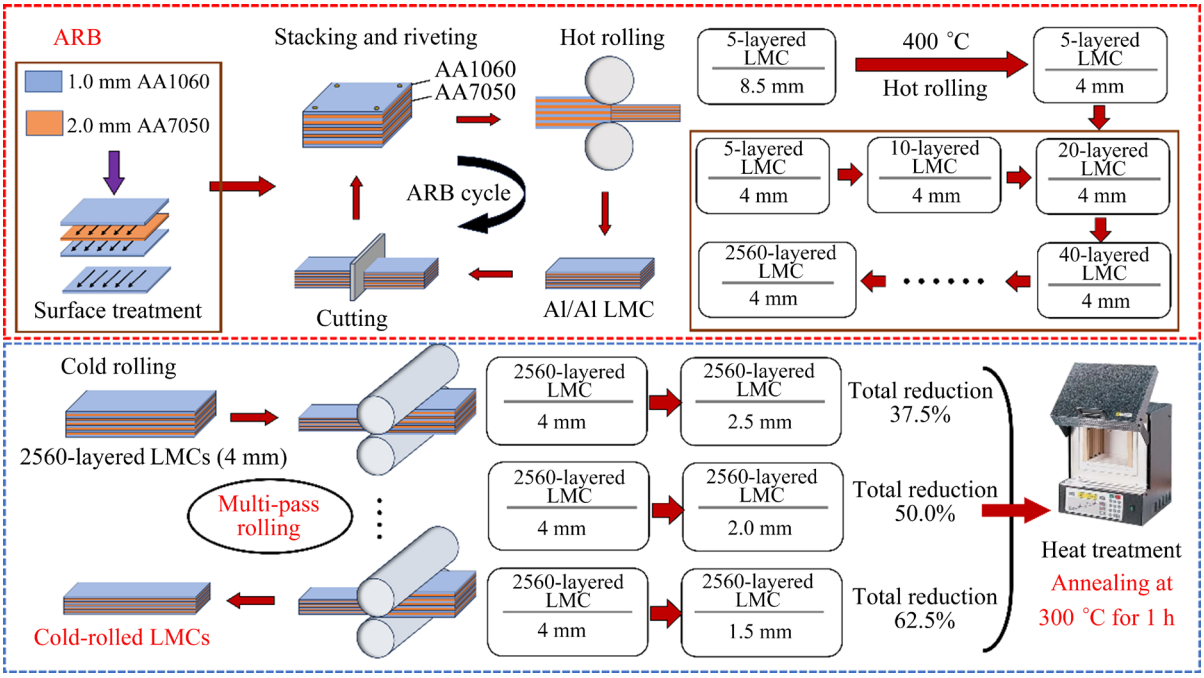

Fig. 2 Schematic illustration of fabrication of Al/Al LMCs

9 cycles until a 2560-layered Al/Al LMC was prepared. (2) Cold rolling and annealing: After the ARB process, the 2560-layered Al/Al LMCs were subjected to three cold rolling processes with total reductions of 37.5%, 50% and 62.5%. In addition, three types of cold-rolled samples were annealed at 300 °C for 1 h to construct heterogeneous lamellar structures, and the effects of annealing on the microstructural and mechanical properties of multilayered LMCs were explored. All heating processes were conducted without a protective atmosphere.

2.2 Microstructural characterization

EBSD was conducted via field-emission scanning electron microscopy (SEM) to examine the microstructural evolution and crystallographic orientation characteristics of the LMCs. The interfacial structures of the LMCs were analyzed via SEM and energy-dispersive X-ray spectroscopy (EDS). After grinding and mechanical polishing, the EBSD specimens were electropolished in an alcohol solution of 10 vol.% perchloric acid at a temperature of −20 °C and an applied voltage of 20 V. The influence of the microstructural

characteristics of the constituent layers on the mechanical properties of the LMCs were further investigated using the transmission electron microscopy (TEM). The specimens for TEM were twin-jet electropolished using 700 mL CH_3OH + 300 mL HNO_3 solution at −30 °C and 20 V polishing voltage.

2.3 Mechanical property tests

The mechanical properties of the LMCs were evaluated via tensile testing at a strain rate of 1.1×10^{-3} s^{-1}. Tensile samples with a gauge area of 18 mm (length) × 5 mm (width) were processed along the rolling direction, and each test was repeated on at least three samples to ensure data reproducibility. To reveal the fracture behaviors and interfacial effects of multilayered LMCs, in situ SEM tensile testing of the annealed Al/Al LMC was carried out inside a tungsten filament SEM instrument equipped with a Gatan™ microtest tensile platform. Then, a specimen with a gauge length of 2 mm and a width of 1.5 mm was machined by mechanical polishing and ion cutting. Furthermore, the differences in the flow properties of the constituent layers were examined by Vickers hardness tests at room temperature, and hardness measurements were carried out using a load of 25 g with a dwelling time of 10 s.

3 Results and discussion

3.1 Microstructural evolution of Al/Al LMCs after ARB

Interfacial morphologies and corresponding microstructures of the constituent layers in the 5-layered Al/Al LMC are shown in Fig. 3. The layer interfaces between the 1060 and 7050 constituents are straight and continuous, revealing that the severe plastic deformation generated by the first ARB process does not lead to plastic instability, as shown in Fig. 3(a). Figures 3(b, c) present the changes in the microstructures of the constituent layers. The differences in the initial material characteristics result in differences in the microstructures of the 1060 and 7050 layers after hot rolling. The more significant grain refinement

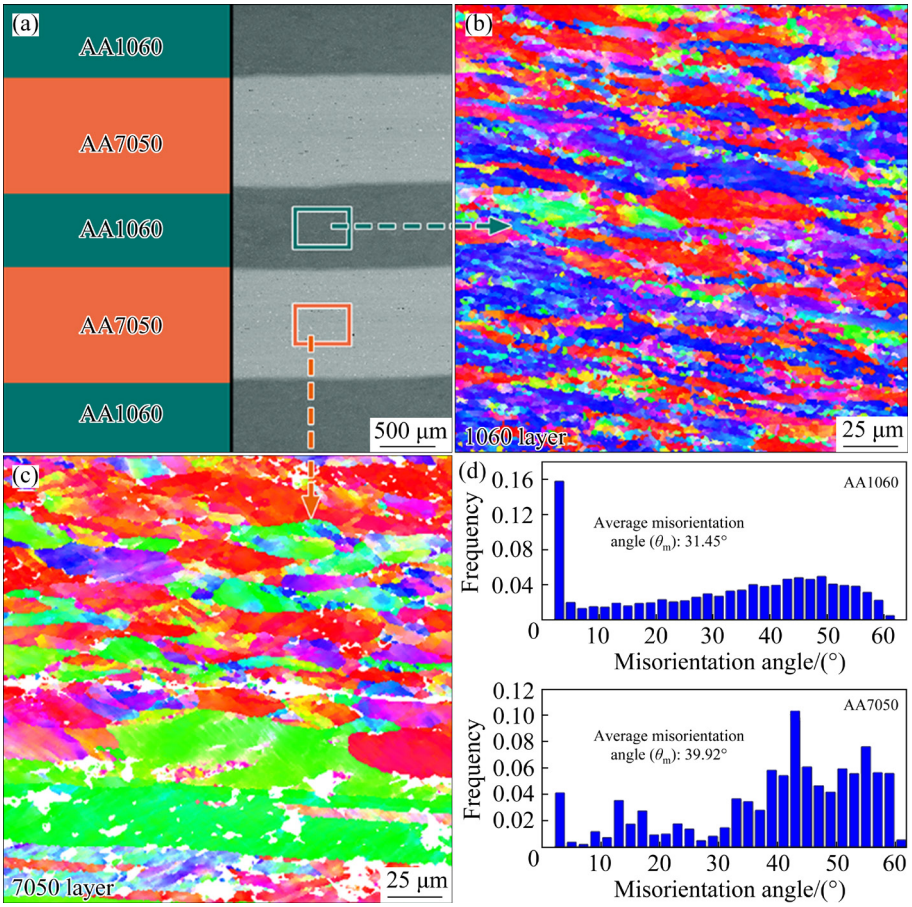

Fig. 3 Interfacial morphologies (a) of 5-layered Al/Al LMC and corresponding microstructures of constituent layers (b, c); Misorientation angles in AA1060 and AA7050 layers for 5-layered specimen (d)

in the 1060 layer compared to that in the 7050 layer is mainly attributed to its greater plasticity. Meanwhile, the difference in flow properties between constituent metals during the repeated deformation of ARB process leads to the formation of interfacial shear, contributing to further refinement of the soft layer of 1060 [19,20]. Based on analysis of the misorientation angles obtained from the EBSD results (Fig. 3(d)), significant differences in the percentages of high- and low-angle grain boundaries of the two constituent metals after plastic deformation are found, indicating the different flow properties of the 1060 and 7050 layers.

Furthermore, the hardness results along the thickness direction of the 5-layered Al/Al LMC provide an intuitive view of the differences in the flow properties of the constituent metals (Figs. 4(a, b)), which is conducive to evaluating the impact of the ARB process on the microstructural and mechanical properties of LMCs under additional cycles and high cumulative strain. Notably, from the energy-dispersive X-ray spectroscopy (EDS) results in the enlarged images of Fig. 4(a), the presence of Mg at the interface position shows a progressive upward trend from the 1060 layer to the 7050 layer, revealing the occurrence of element diffusion behavior induced by strain and temperature fields during the hot rolling process. This result indirectly indicates that excellent interfacial metallurgical bonding is achieved between dissimilar aluminum alloys.

Figure 5 shows the interfacial evolution of the Al/Al LMCs after performing various ARB

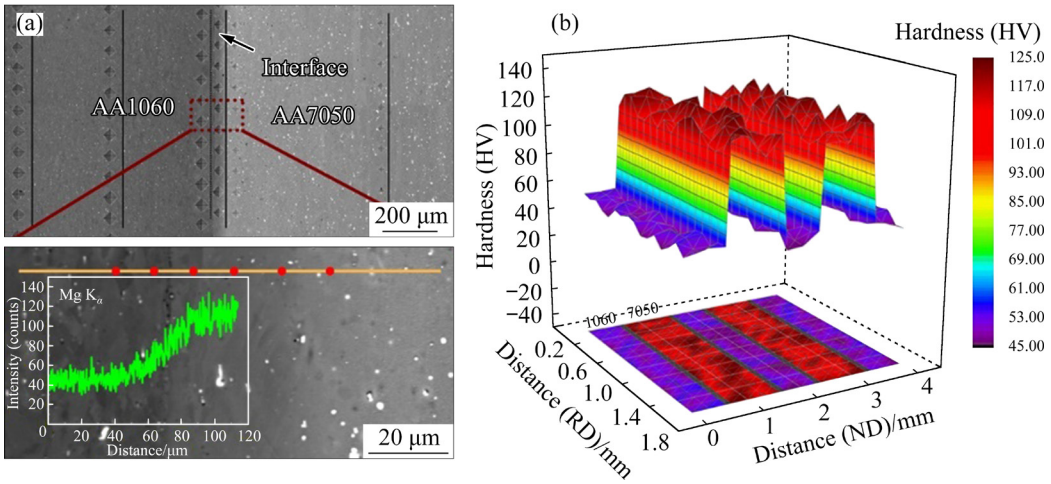

Fig. 4 Elemental distribution (a) and Vickers hardness (b) along interface of 5-layered Al/Al LMC

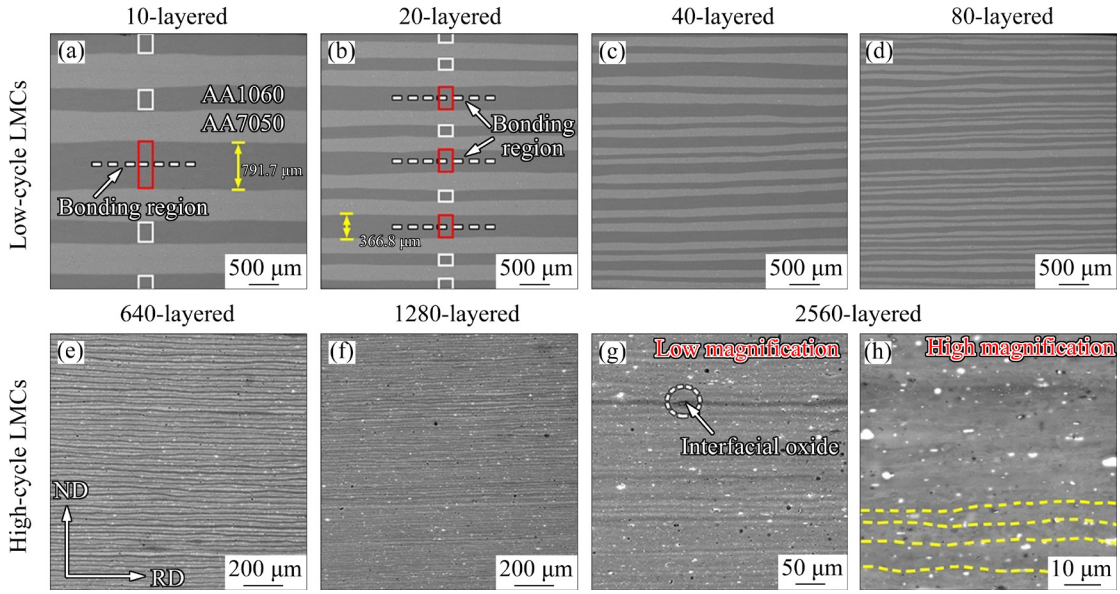

Fig. 5 Interfacial morphologies of ARB Al/Al LMCs

processes. As shown in Figs. 5(a, b), the thickness variation in the soft layer of 1060 after rolling deformation is significantly greater than that in the hard layer of 7050. In addition, the bonding interface is defined by the thicknesses of the red boxes being greater than those of the 1060 layers. In the low-cycle ARB LMCs (Figs. 5(a−d)), the interface is continuous, and signs of oxide generation are difficult to detect; moreover, the existence of interfacial oxides can be observed in the microstructure of the 2560-layered Al/Al LMC (Fig. 5(g)). This finding is attributed to the inevitable oxidation of the bonding surface caused by repeated heating processes after 9 ARB cycles. In general, due to differences in the flow properties between constituent layers, the interfacial shear effect under severe plastic deformation leads to obvious plastic instability in laminated composite materials. Related studies on Ti/Cu [21], Mg/Al [22], Cu/Ta [8], and other composites have been extensively reported. Interestingly, obvious local necking or fracture cannot be detected in the 1060/7050 LMCs with an increase in the number of layers, even for high-cycle ARB (Figs. 5(e−h)), mainly due to dynamic recrystallization during high-temperature ARB processes [8].

During the observation of the interface morphology of the 2560-layered Al/Al LMC (Fig. 5(g)), the ultrahigh number of constituent layers makes distinguishing the interface structure difficult, and the existence of the interface can be distinguished based only on the microstructural characteristics (i.e., the second-phase particles or crystals) from the high-magnification image shown in Fig. 5(h).

To further reveal the interfacial and microstructural details of the constituent metals in the ultrahigh-layered samples, the TEM morphology of the 2560-layered Al/Al LMC was obtained, as shown in Fig. 6. Figure 6(b) shows that the thickness of Layer 1060 in the 2560-layered Al/Al LMC is approximately 2.9 μm. Under dynamic recrystallization during hot rolling, the microstructure is mostly dominated by substructures with sharp boundaries, and the grain morphology exhibits an obvious mixed distribution of equiaxed and elongated crystals (Fig. 6(c)). Conversely, the considerable second-phase particles distributed in the matrix indicate the direction for distinguishing the 7050 layers. The microstructure of the sample with a layer thickness of 4.4 μm is basically characterized by nanoscale elongated grains. Figure 6 reveals that, except for the changes in size, microstructure development in the constituent layers of the 2560-layered LMC remains the same as that in the low-cycle ARB, as shown in Fig. 3.

3.2 Construction of heterogeneous lamellar structure and its effect on mechanical properties

To emphasize the influences of reinforced structures on the microstructural and mechanical properties of Al/Al LMCs, different deformation conditions (i.e., the rolling reductions of 37.5%,

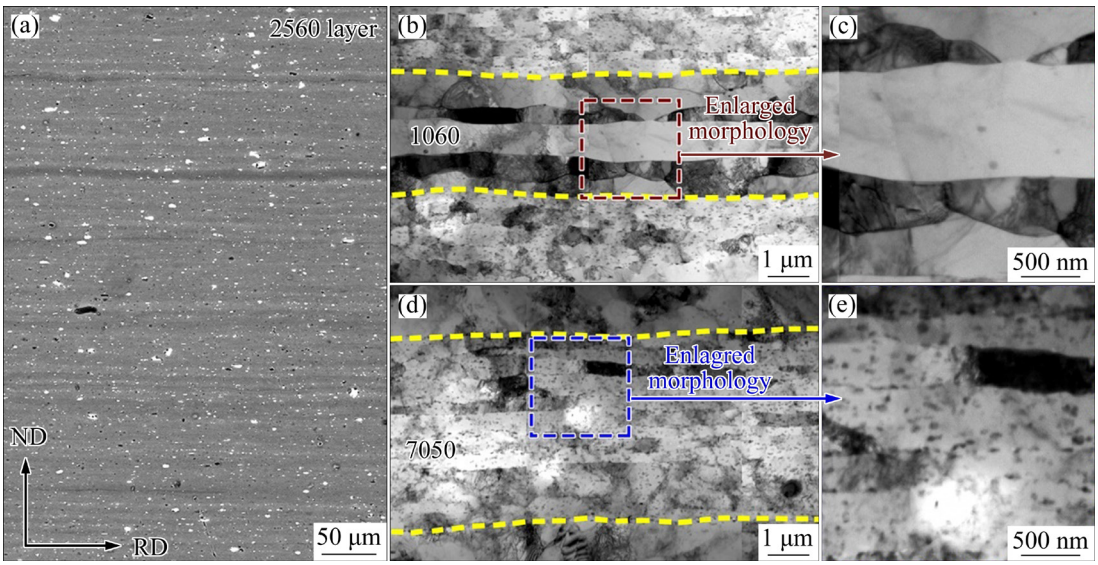

Fig. 6 SEM image showing alternating constituents in 2560-layered specimen (a); Typical cross-sectional TEM images of AA1060 layer (b, c); Typical cross-sectional TEM images of AA7050 layer (d, e)

50.0% and 62.5%) were applied in conjunction with annealing treatment (300 °C, 1 h) to construct heterogeneous lamellar structures in the 2560-layered LMC. Figure 7 shows the mechanical properties of the 2560-layered Al/Al LMCs under various processing conditions. As shown in Fig. 7(a), due to the changes in the mechanical properties of the as-rolled specimens, the strain hardening behavior significantly increases the strength of the Al/Al LMC with increasing rolling reduction, while the elongation gradually decreases. After annealing at 300 °C for 1 h, all the as-rolled samples soften simultaneously, and the recovery and recrystallization under the high-temperature conditions decreased the strength of the Al/Al LMC while significantly improve its ductility.

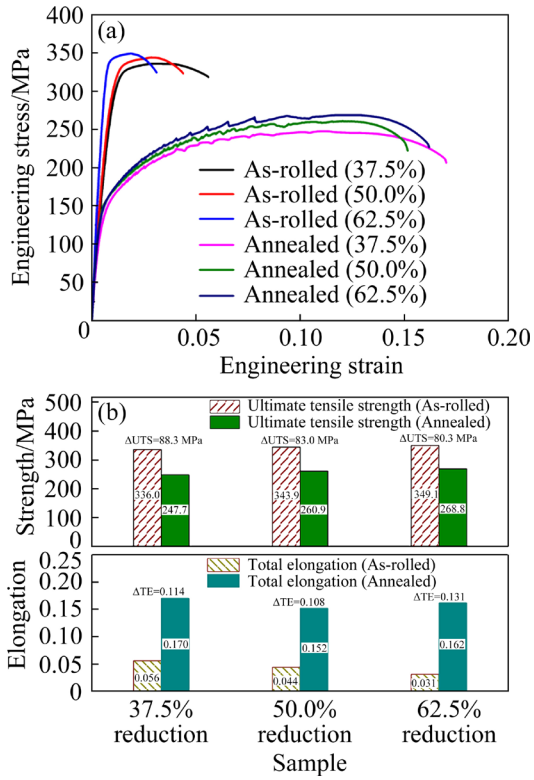

Fig. 7 Engineering stress–strain curves of 2560-layered Al/Al LMC under various process conditions (a); Strength and elongation before and after annealing (b)

Interestingly, the plastic deformation ability of the 62.5% reduction specimen exhibits an abnormal evolution after annealing treatment, with a greater elongation than that of the 50.0% reduction specimen. Correspondingly, the development of strength and elongation before and after annealing is summarized in Fig. 7(b), revealing that the best combination of strength and ductility can be achieved in the 62.5% reduction specimen after annealing. This finding suggests that an unusual plastic deformation process occurs in the 62.5% reduction specimen, which may be attributed to the interfacial effect between layers during tensile testing.

Figure 8 presents a comprehensive comparison of the microstructures of the various annealed specimens, with an emphasis on grain differences in the constituent layers. Various types of boundaries, including high-angle grain boundaries (HAGBs) and low-angle grain boundaries (LAGBs), are defined by black and gray lines, respectively. The excellent bonding at the layer interfaces can be easily observed in Fig. 8, and the microstructural distribution of the constituent layers varies significantly depending on the annealing state. As shown in Figs. 8(a−c), the change in the degree of deformation before annealing impacts the microstructural changes in the Al/Al LMC, which is mainly reflected in the differences in the degree of recrystallization between the constituent layers. The microstructure of the 37.5% annealed sample basically recrystallizes, and the grains in the 1060 and 7050 layers are difficult to distinguish (Fig. 8(a)). However, as the rolling reduction before annealing increases to 50% and to 62.5% (Figs. 8(b) and 8(c), respectively), the increase in the degree of deformation results in some of the microstructures in the 7050 layers remaining deformed at 300 °C, and the percentage of these layers gradually increases. Understandably, the increase in the number of deformed structures in the Al/Al LMC under a larger rolling reduction, such as grain refinement and dislocation cell formation, delays the recovery and recrystallization of microstructures during annealing. In addition, the difference in recrystallization temperature between AA1060 and AA7050 is considered the main reason why the characteristics of some of the deformed grains of the 7050 layers do not change.

Notably, in Fig. 8(c), a typical heterogeneous lamellar structure can be observed in the 62.5% reduction specimen, and a significant microstructural difference is detected in the 1050 and 7050 layers from the enlarged morphology in Fig. 8(d). Additionally, the quantitative analysis of the relative misorientation reveals the formation of a considerable strain gradient at the interface between the 1060 and 7050 layers. Generally,

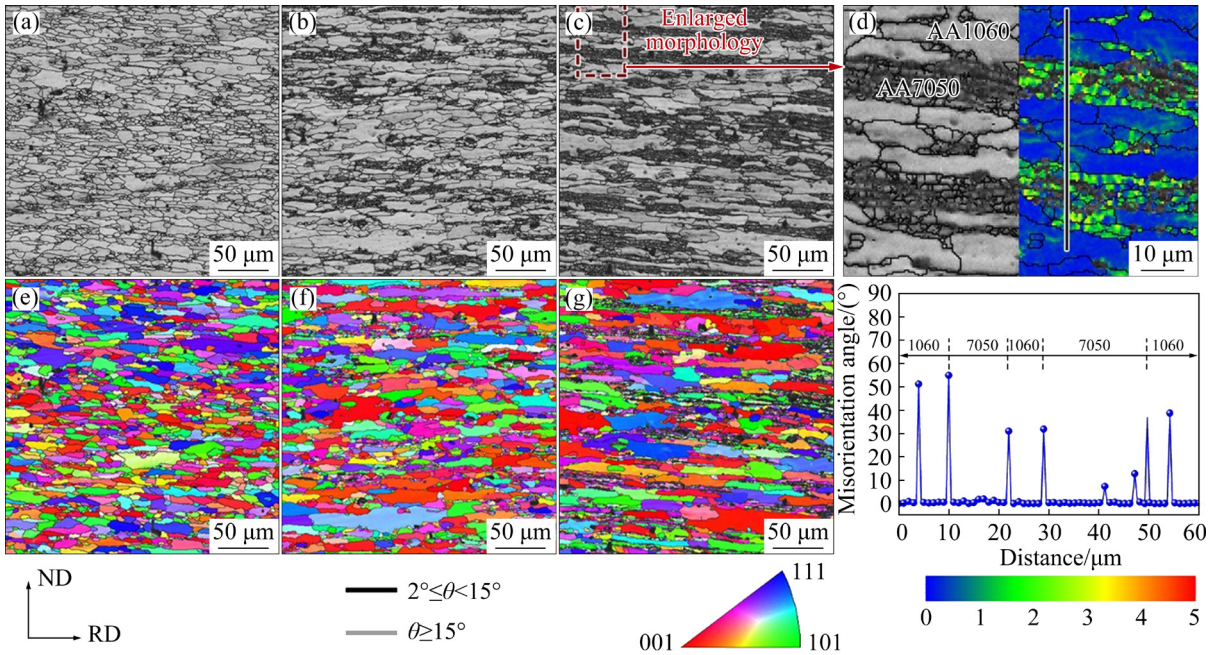

Fig. 8 Microstructural evolution (a−c) and inverse pole figure (IPF) (e−g) of 2560-layered Al/Al LMCs after annealing treatment: (a, e) 37.5% reduction specimen; (b, f) 50.0% reduction specimen; (c, g) 62.5% reduction specimen; (d) Corresponding enlarged morphologies and relative misorientation profiles along black line

during the deformation of a heterogeneous lamellar structure, the strain gradient near the interface, which is caused by the incompatible deformation between dissimilar constituents, promotes the accumulation of GNDs, leading to a complex stress state near the interface and extraordinary strain hardening [23]. Therefore, the better mechanical properties of the 62.5% reduction sample compared to those of the other samples mainly depend on the additional strengthening effect and strain hardening ability introduced by the heterogeneous lamellar structure. Conversely, from the inverse pole figure (IPF) shown in Figs. 8(e−g), the changes in the crystal orientations of the three annealed samples are basically the same and are discretely distributed without the formation of typical textures.

The recrystallized, substructured and deformed microstructures of the 2560-layered Al/Al LMCs under various conditions were analyzed via EBSD, as shown in Fig. 9. Specifically, the recrystallized, substructured and deformed microstructures of the Al layer under various conditions were processed according to the average internal misorientation angle within grains (the minimum misorientation angles of "subgrains" and "grains" were determined to be 2° and 15°, respectively). As shown in Fig. 9(a), a recrystallized structure comprises the majority of the microstructure in the 37.5% reduction specimen, and only a few deformed microstructures can be observed. With increasing rolling reduction before annealing (Figs. 9(b, c)), the percentages of substructures and deformed structures in the 2560-layered Al/Al LMC gradually increase. In addition, the microstructure in the 62.5% reduction sample is basically dominated by substructures.

In fact, the microstructural evolution after annealing is mainly determined by grain refinement before deformation and recrystallization induced by high temperatures. Therefore, the microstructure of the Al/Al LMC under severe plastic deformation with 62.5% reduction mainly exhibits typical substructural characteristics after the annealing treatment. Additionally, for the 62.5% reduction specimen, microstructural distribution composed of large-area substructures and deformed fine grains embedded in the substructures clearly indicates the formation of heterogeneous lamellar structures, which is consistent with the previous analysis in Fig. 8.

Figures 10(a−d) and 10(e−h) show the TEM images of the 2560-layered Al/Al LMCs with a 62.5% rolling reduction before and after annealing treatment, respectively. For comparison, the

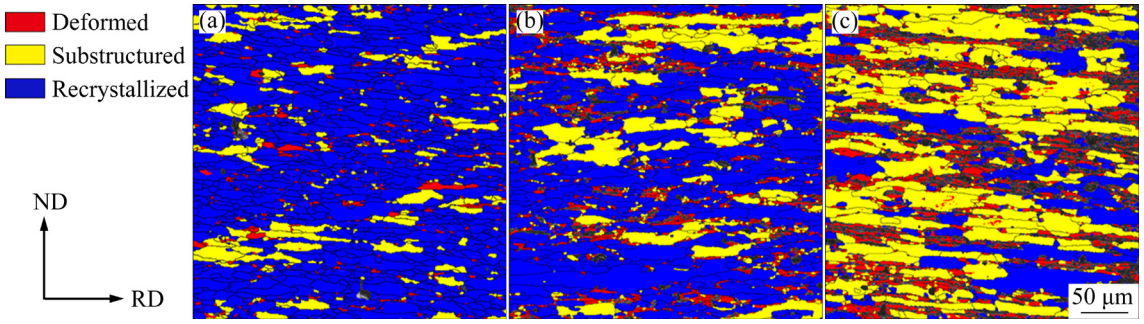

Fig. 9 Recrystallized, substructured and deformed microstructures of 2560-layered LMCs after annealing treatment: (a) 37.5% reduction specimen; (b) 50.0% reduction specimen; (c) 62.5% reduction specimens

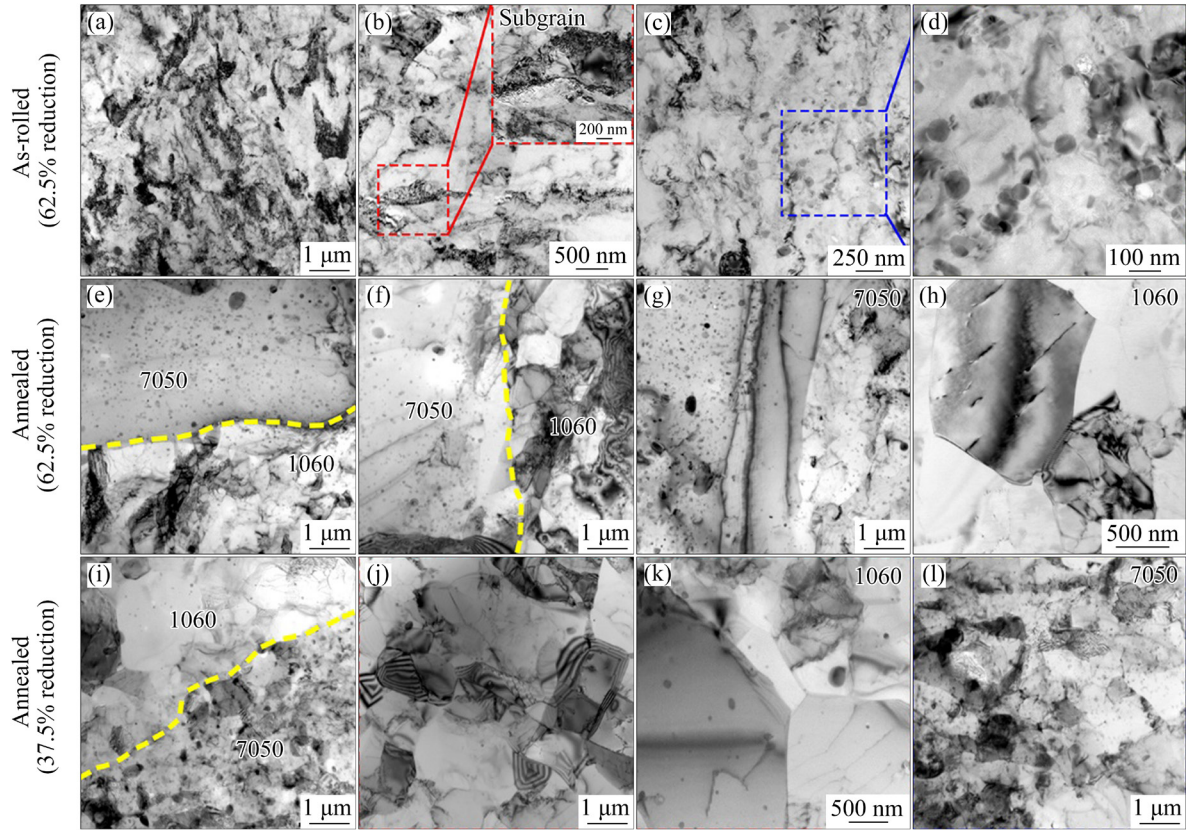

Fig. 10 TEM images of 2560-layered Al/Al LMCs under various conditions

microstructures of the 2560-layered Al/Al LMC with a 37.5% rolling reduction after annealing are shown in Figs. 10(i−l). As shown in Figs. 10(a, b), few second-phase particles present in the 1050 layer. In addition, a high density of dislocations and a large fraction of subgrains indicate severe plastic deformation of the 1050 layer after cold rolling, corresponding to a 62.5% reduction. In the 7050 layer (Fig. 10(c)), the distributions of second-phase particles after rolling are dense, and their morphologies are mainly dominated by spherical and rod-like shapes (as shown in the enlarged morphology in Fig. 10(d)). In general, these dispersoid particles are confirmed to be Cr- or Mn-containing particles [24].

The microstructural evolution of the 2560-layered Al/Al LMC with a 62.5% reduction after annealing treatment is the focus of mechanical property optimization, as shown in Fig. 7. Interestingly, the differences in the microstructural characteristics of the 1060 and 7050 layers after annealing make it easy to distinguish the interfaces between the constituent layers, as shown in Figs. 10(e) and 10(f), respectively. Specific TEM images of the constituent layers indicate that the distribution of the second-phase particles

precipitated from the 7050 layer is dense and uniform under the high-temperature conditions (Fig. 10(g)). Additionally, although annealing decreases the dislocation density, the crystal structure shows little tendency toward the recrystallization and an equiaxed state in the 7050 layers. In contrast, the enlarged morphology of the 1060 layer shown in Fig. 10(h) indicates that the internal dislocation densities of substructures for the as-rolled specimen decrease, and the substructures gradually develop toward an equiaxed state after annealing at 300 °C. However, the microstructure observed in the 1060 layer indicates that the substructures are still dominant and the recrystallization is incomplete after annealing, which is consistent with the analysis shown in Fig. 9(c). Microstructural details reveal that during annealing at 300 °C, after cold rolling with 62.5% reduction, the 2560-layered Al/Al LMC can increase the differences in the flow properties of the constituent layers based on the reasonable regulation of deformation and recrystallization processes, effectively constructing a heterogeneous lamellar structure. The above TEM analyses verify the EBSD results in Fig. 8.

The incompatible deformation caused by large differences in flow properties between the 1060 and 7050 layers leads to the formation of strain gradients, providing additional strengthening for Al/Al LMCs and optimizing their mechanical properties. Conversely, for the 37.5% reduction specimen, the layer interface is easily determined based on the distribution of second-phase particles (Fig. 10(i)). Although the microstructure of the 1060 layers after annealing with 37.5% reduction is completely recrystallized (Figs. 10(j, k)), the development of a deformed structure toward equiaxed grains after annealing can be observed in the 7050 layers (Fig. 10(l)), indicating that the differences in the flow properties of the constituent layers are less than those for the Al/Al LMC after annealing with 62.5% reduction. According to the theory of back stress strengthening, the incompatible deformation caused by differences in flow properties during plastic deformation is the main reason for the formation of strain gradients [13,23]. That is, the additional strengthening provided by the 37.5% reduction specimen with low differences in flow properties between the 1060 and 7050 layers is lower than that provided by the 62.5% reduction specimen, which is considered the main reason why the combination of strength and ductility in the Al/Al LMC after annealing with 62.5% reduction is better than that in the other specimens.

3.3 Deformation mode and fracture behavior of constituent layers

Figure 11 shows the fracture details during the in-situ SEM tensile test of 62.5% reduction specimen of Al/Al LMC after annealing treatment. Interestingly, when the strain increases to 5.8% (Fig. 11(a)), the soft layer of 1060 exhibits significant deformation and slip band generation. Conversely, the hard layer of 7050 remains unchanged, revealing the initiation of plastic deformation after the yielding of the 2560-layered Al/Al LMC. According to classical dislocation theory, a close relationship exists between dislocations and slip; i.e., dislocations are the basis of slip occurrence, and slip is the result of dislocation motion. In the plastic deformation stage

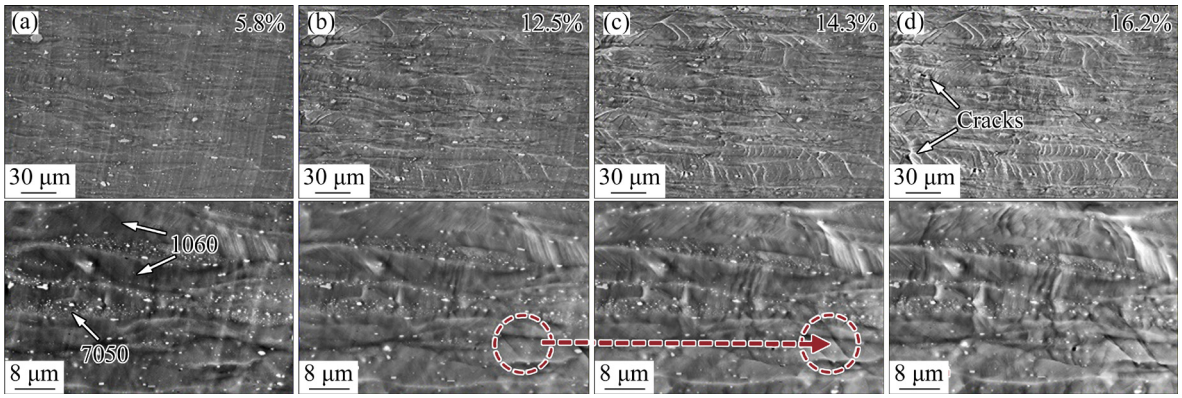

Fig. 11 Fracture surface morphologies during in-situ SEM tensile test at different strain levels of 62.5% reduction specimen of Al/Al LMC after annealing treatment: (a) 5.8%; (b) 12.5%; (c) 14.3%; (d) 16.2%

of the 62.5% reduction specimen, the slip system in the soft layer is activated first, indicating that dislocations first occur in the 1060 constituents, which is consistent with the findings of the previous analysis on the generation of strain gradients under incompatible deformation.

As shown in Fig. 11(b), a further increase in strain leads to an increase in plastic deformation, and the codeformation throughout the entire composite produces a typical shear band occurring mostly at a 45° angle from the rolling direction (marked by the red circle in Fig. 11), revealing that necking and possibly fracture might develop at these positions [25]. Furthermore, no obvious deformation is observed in the 7050 layer when the strain reaches 12.5%. However, when the strain increases from 12.5% to 14.3%, the shear band that originates in the 1060 layer crosses the interface and extends toward the 7050 layers, inducing deformation and subsequent fracture of the hard layer, as shown in Fig. 11(c). During plastic deformation, the soft layer of laminated composites is likely responsible for accommodating the deformation, while the hard layer serves as the main load-bearing phase [26]. When the strain of the 2560-layered LMC exceeds the uniform elongation, the soft layer of 1060 reaches its strength limit, inducing deformation to continue to develop toward the hard layer of 7050. Additionally, although the main crack does not propagate to the selected position after complete fracture of the Al/Al LMC, some microcracks originating from the second-stage particles or layer interface can be detected in Fig. 11(d).

To emphasize the fracture evolution in 62.5% reduction specimen of Al/Al LMC after annealing treatment, the initiation and propagation of cracks at various stages during the tensile process are presented in Fig. 12. No significant changes are observed in the microstructure during the elastic stage (Stage I). However, when the LMC reaches to the plastic deformation stage (Stage II), local deformation and necking caused by stress concentration are observed, indicating that cracks are likely to initiate after the strength limit of the Al/Al LMC is reached, as shown in Stage III. In addition, the aggravation of deformation leads to crack propagation and crossed shear band formation as the strain further increases (Stage IV). Finally, complete fracturing occurs at the largest crack of the Al/Al LMC. Notably, Fig. 12 shows the continuous stress–strain curve without the segmentation. Accordingly, the interface of the 2560-layered Al/Al LMC after ARB has excellent bonding, which is beneficial to expanding the range of applications guided by the interface structure, such as exposure to high-velocity impact or chemical corrosion.

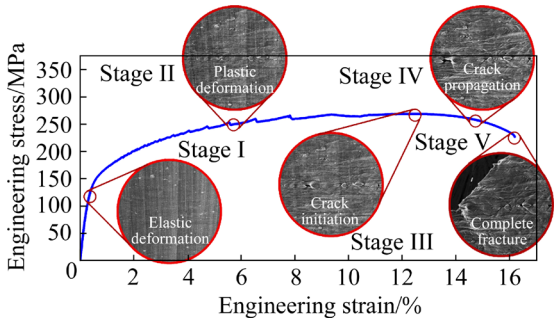

Fig. 12 Crack evolution at different stages for 62.5% reduction specimen of Al/Al LMC after annealing treatment during in-situ SEM tensile testing

3.4 Contribution of back stress strengthening to mechanical properties

The strain gradient introduced by the mechanical incompatibility between constituent layers after annealing treatment is the key factor causing additional strengthening effects (i.e., back stress strengthening) on the mechanical properties of the Al/Al LMC. Back stress, as a type of long-range stress, has been reported to play a major role in additional strengthening behaviors [13,18]. In this regard, loading–unloading–reloading (LUR) tests were conducted to study the influence of back stress on the mechanical properties of 2560-layered Al/Al LMCs after annealing treatment.

Figure 13(a) shows the true stress–strain curves for the LUR tests on all annealed specimens with various rolling reductions, and magnified views of the typical hysteresis loops at different predetermined strains for the 62.5% reduction specimen are highlighted in Fig. 13(b). In general, the back stress (σ_b) can be estimated by the average values of the unloading (σ_r) and loading (σ_u) yield stresses ($\sigma_b=(\sigma_r+\sigma_u)/2$) [23], and the corresponding parameters in the hysteresis loop are shown in Fig. 13(c). On this basis, the evolution of the back stress as a function of the applied tensile strain can be calculated from the hysteresis loops at various tensile strains and is plotted in Fig. 13(d). The

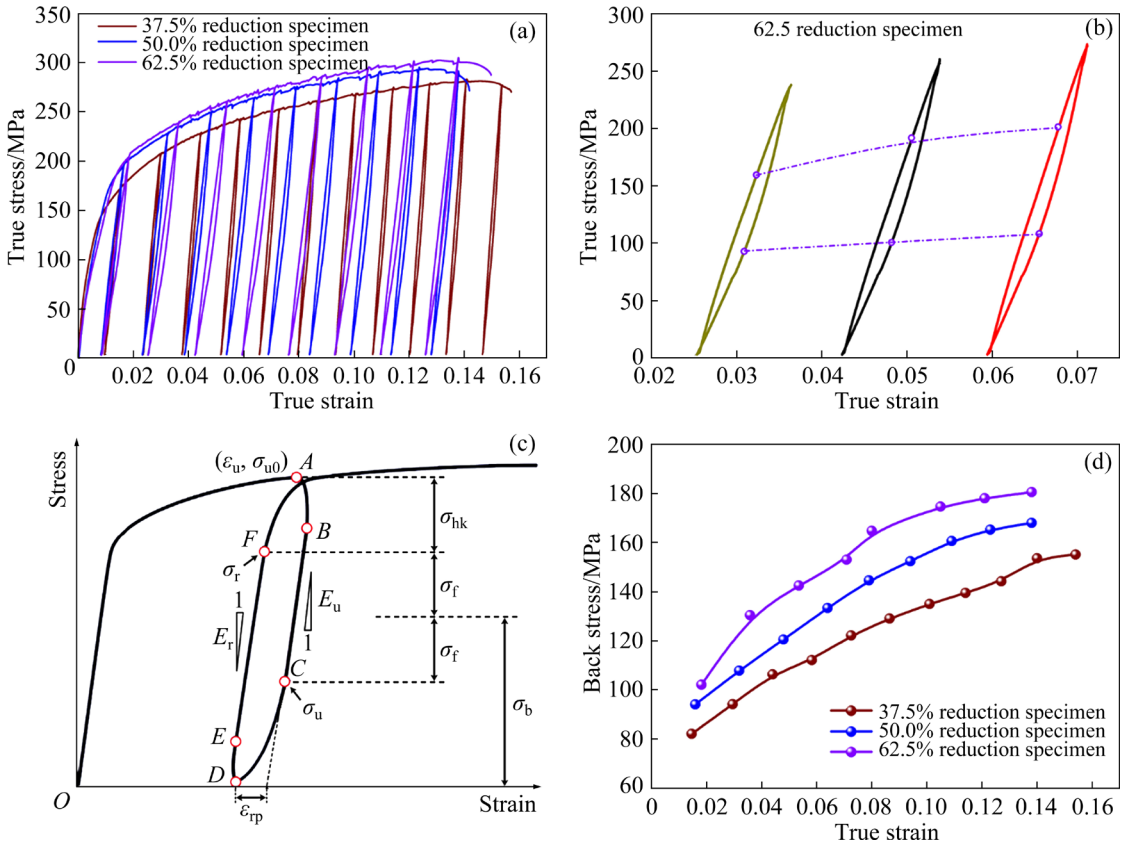

Fig. 13 Unloading–reloading stress–strain curves of 2560-layered Al/Al LMCs with various reductions (a); Magnified view of typical hysteresis loops (b); Schematic for calculating back stress (c); Evolution of back stress with increasing applied strain (d)

quantitative results reveal that the back stress of the 62.5% reduction specimen is far greater than that of the other specimens at all tensile strains, indicating that more considerable extra strengthening and strain hardening effects present in the 62.5% reduction Al/Al LMC. According to the evolution of the microstructure in the constituent layers (Figs. 8 and 10), the differences in flow properties between the 1060 and 7050 layers in the annealed Al/Al LMC after 62.5% cold rolling are greater than those in the other layers, with 37.5% and 50% reductions, respectively. Consequently, the increase in the back stress in the 62.5% reduction specimen is primarily due to the high magnitude of incompatibility during tensile deformation.

To further reveal the mechanism underlying the generation of back stress, Fig. 14 shows the accumulation of GNDs at the layer interface in 1060/7050 LMCs with heterogeneous lamellar structures. Figures 14(a, b) present a schematic diagram of a microstructure similar to that of the 62.5% reduction specimen after annealing treatment, which is mainly composed of lamellar structures with elongated ultrafine-grained domains embedded in a coarse-grained matrix. Correspondingly, a smooth strain curve is shown that varies with distance from the interface in Fig. 14(c), and the other curve in represents the corresponding strain gradient. Obviously, the accumulation of GNDs generates strain and stress gradients near the interface under incompatible deformation between the constituent layers (Fig. 14(d)), which is considered the main reason for the formation of back stress strengthening and strain hardening.

Based on the microstructural analysis of the annealed LMCs shown in Fig. 8, it is reasonable to presume that with the increased magnitude of incompatibility in the heterogeneous lamellar structure, the density of the GNDs increases to accommodate the larger strain gradient, leading to more considerable back stress strengthening and improved mechanical properties. Therefore, this investigation provides a feasible perspective for the preparation of heterogeneous lamellar structures,

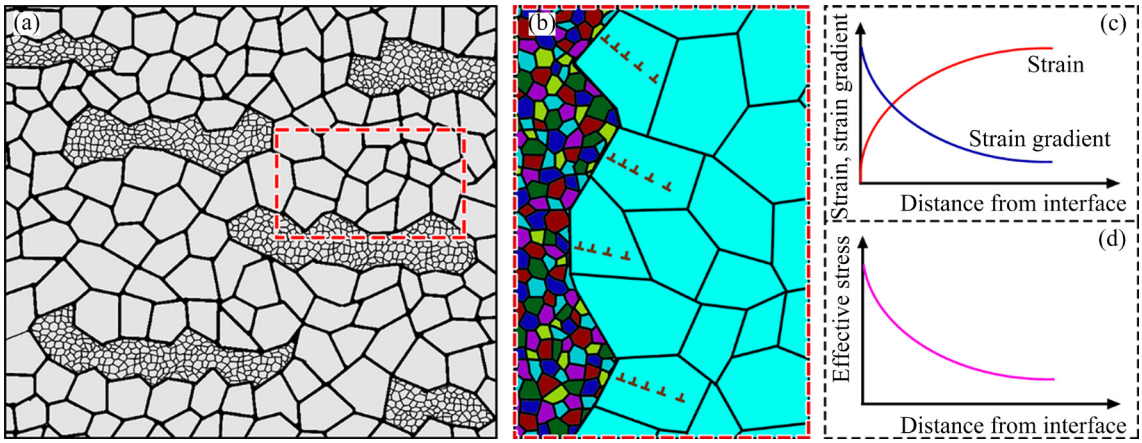

Fig. 14 Schematics of lamellar structures with elongated ultrafine-grained domains embedded in coarse-grained matrix (a); Accumulation of geometrically necessary dislocations from magnified area (b); Plastic strain and strain gradient (c); Effective stress as function of distance from domain interface (d)

which is beneficial to the structural design of the laminated metal composites with excellent performance.

4 Conclusions

(1) 2560-layered Al/Al LMC was successfully prepared by the ARB process, and plastic instability under high-temperature conditions is suppressed, promoting the maintenance of a straight and continuous state at the interface for most ARB cycles.

(2) Differences in the flow properties between the 1060 and 7050 constituents are observed in the low- and high-ARB cycle samples, which is mainly attributed to differences in microstructure, such as the distributions of second-phase particles, crystal sizes and morphologies, under severe plastic deformation.

(3) After annealing at 300 °C for 1 h, the cold-rolled 2560-layered Al/Al LMC with 62.5% reduction exhibits the best combination of strength and ductility among the specimens. This finding reveals that the additional strain hardening and back stress strengthening effects introduced by mechanical incompatibility contribute to the optimization of the mechanical properties.

(4) With the increased magnitude of incompatibility in the 2560-layered Al/Al LMC with a heterogeneous lamellar structure, the densities of the GNDs increase to accommodate the larger strain gradient, resulting in more considerable back stress strengthening and improved mechanical properties.

CRediT authorship contribution statement

Tai-qian MO: Conceptualization, Methodology, Data curation, Writing − Original draft, Software; **Hua-qiang XIAO:** Investigation, Methodology, Resources; **Cun-hong YIN:** Resources, Data curation, Writing − Review & editing, Funding acquisition; **Bo LIN:** Validation, Formal analysis, Writing − Review & editing, Supervision, Funding acquisition; **Xue-jian WANG:** Methodology, Investigation, Visualization; **Kai MA:** Conceptualization, Supervision, Project administration.

Declaration of competing interest

The authors declare that they have no known competing financial interests or personal relationships that could have appeared to influence the work reported in this paper.

Acknowledgments

The authors are grateful for the financial support from the Special Fund for Special Posts of Guizhou University, China (No. [2022]06), the Guizhou Provincial Basic Research Program (Natural Science), China (No. ZK [2023]78), the National Natural Science Foundation of China (No. 52365020), and the Open Fund Project of Key Laboratory of Advanced Manufacturing Technology, China (No. GZUAMT2022KF [04]).

References

[1] KALANTARRASHIDI N, ALIZADEH M, PASHANGEH S.

Consideration on zinc content on the microstructure, mechanical, and corrosion evolution of aluminum/zinc composites fabricated by CARB process [J]. Journal of Materials Research and Technology, 2022, 19: 1805−1820.

[2] ZHU Guo-chuan, LI Xi-wu, XIONG Bai-qing, LI Zhi-hui, ZHANG Yong-an, YAN Li-zhen, WEN Kai-yan, YAN Hong-wei. Dynamic response characteristic of 7N01/7A01/7050 aluminium multilayer plate at high strain rate [J]. Progress in Natural Science−Materials International, 2021, 31(1): 159−163.

[3] ABBASI M, TOROGHINEJAD M R. Effects of processing parameters on the bond strength of Cu/Cu roll-bonded strips [J]. Journal of Materials Processing Technology, 2010, 210(3): 560−563.

[4] LI Shun-qiang, SUN Guo-sheng, ZHANG Rui-sheng, CHENG Xiao, LIU Ji-zi. Effect of heat treatment on microstructure and mechanical property of roll-bonded 1060/7N01/1060 laminates [J]. Transactions of Nonferrous Metals Society of China, 2024, 34: 94−107.

[5] YU H L, LU C, TIEU A K, LI H J, GODBOLE A, KONG C. Annealing effect on microstructure and mechanical properties of Al/Ti/Al laminate sheets [J]. Materials Science and Engineering A, 2016, 660: 195−204.

[6] MO Tai-qian, CHEN Ze-jun, ZHOU Zhan-song, LIU Jiang-jiang, HE Wei-jun, LIU Qing. Enhancing of mechanical properties of rolled 1100/7075 Al alloys laminated metal composite by thermomechanical treatments [J]. Materials Science and Engineering A, 2021, 800: 140313.

[7] ZHANG Jian-yu, WANG Yan-hui, LV Zheng, CHEN Qing-an, CHEN Ya-yu, LI He-zong. Formation mechanism and growth kinetics of $TiAl_3$ phase in cold-rolled Ti/Al laminated composites during annealing [J]. Transactions of Nonferrous Metals Society of China, 2022, 32: 524−539.

[8] ZENG L F, GAO R, FANG Q F, WANG X P, XIE Z M, MIAO S, HAO T, ZHANG T. High strength and thermal stability of bulk Cu/Ta nanolamellar multilayers fabricated by cross accumulative roll bonding [J]. Acta Materialia, 2016, 110: 341−351.

[9] MA X L, HUANG C X, MOERING J, RUPPERT M, HOPPEL H W, GOKEN M, NARAYAN J, ZHU Y T. Mechanical properties of copper/bronze laminates: Role of interfaces [J]. Acta Materialia, 2016, 116: 43−52.

[10] WANG Shuai, HUANG Lu-jun, JIANG Shan, ZHANG Rui, SUN Feng-bo, AN Qi, GENG Lin. Multiplied bending ductility and toughness of titanium matrix composites by laminated structure manipulation [J]. Materials & Design, 2021, 197: 109237.

[11] LU Ke. Making strong nanomaterials ductile with gradients [J]. Science, 2014, 345(6203): 1455−1456.

[12] NIU G, ZUROB H S S, MISRA R D K, TANG Q, ZHANG Z, NGUYEN M-T, WANG L, WU H, ZOU Y. Superior fracture toughness in a high-strength austenitic steel with heterogeneous lamellar microstructure [J]. Acta Materialia, 2022, 226: 117642.

[13] WU X L, ZHU Y T. Heterogeneous materials: A new class of materials with unprecedented mechanical properties [J]. Materials Research Letters, 2017, 5(8): 527−532.

[14] MA K, LIU Z Y, LIU B S, XIAO B L, MA Z Y. Improving ductility of bimodal carbon nanotube/2009Al composites by optimizing coarse grain microstructure via hot extrusion [J]. Composites Part A, 2021, 140: 106198.

[15] LI Jian-sheng, CAO Yang, GAO Bo, LI Yu-sheng, ZHU Yun-tian. Superior strength and ductility of 316L stainless steel with heterogeneous lamella structure [J]. Journal of Materials Science, 2018, 53(14): 10442−10456.

[16] WU Xiao-lei, YANG Mu-xin, YUAN Fu-ping, WU Gui-lin, WEI Yu-jie, HUANG Xiao-xu, ZHU Yun-tian. Heterogeneous lamella structure unites ultrafine-grain strength with coarse-grain ductility [J]. Proceedings of the National Academy of the Sciences of the United States of America, 2015, 112(47): 14501−14505.

[17] JIANG Y, GU R C, ZHANG Y, WANG J T. Heterogeneous structure controlled by shear bands in partially recrystallized nano-laminated copper [J]. Materials Science and Engineering A, 2018, 721: 226−233.

[18] HE Jin-yan, MA Yan, YAN Ding-shun, JIAO Si-hai, YUAN Fu-ping, WU Xiao-lei. Improving ductility by increasing fraction of interfacial zone in low C steel/304 SS laminates [J]. Materials Science and Engineering A, 2018, 726: 288−297.

[19] QUADIR M Z, FERRY M, AL-BUHAMAD O, MUNROE P R. Shear banding and recrystallization texture development in a multilayered Al alloy sheet produced by accumulative roll bonding [J]. Acta Materialia, 2009, 57: 29−40.

[20] MA M, HUO P, LIU W C, WANG G J, WANG D M. Microstructure and mechanical properties of Al/Ti/Al laminated composites prepared by roll bonding [J]. Materials Science and Engineering A, 2015, 636: 301−310.

[21] JIANG S, PENG R L, JIA N, ZHAO X, ZUO L. Microstructural and textural evolutions in multilayered Ti/Cu composites processed by accumulative roll bonding [J]. Journal of Materials Science & Technology, 2019, 35: 1165−1174.

[22] ZHANG An-xin, LI Feng, HUO Peng-da, NIU Wen-tao, GAO Rong-he. Response mechanism of matrix microstructure evolution and mechanical behavior to Mg/Al composite plate by hard-plate accumulative roll bonding [J]. Journal of Materials Research and Technology, 2023, 23: 3312−3321.

[23] YANG Mu-xin, PAN Yue, YUAN Fu-ping, ZHU Yun-tian, WU Xiao-lei. Back stress strengthening and strain hardening in gradient structure [J]. Materials Research Letters, 2016, 4: 145−151.

[24] LIU S, ZHONG Q, ZHANG Y, LIU W, ZHANG X, DENG Y. Investigation of quench sensitivity of high strength Al−Zn−Mg−Cu alloys by time–temperature-properties diagrams [J]. Materials & Design, 2010, 31: 3116−3120.

[25] GOVINDARAJ N V, FRYDENDAHL J G, HOLMEDAL B. Layer continuity in accumulative roll bonding of dissimilar material combinations [J]. Materials & Design, 2013, 52: 905−915.

[26] ZHOU Qing, ZHANG Suang, WEI Xue-zi, WANG Fei, HUANG Ping, XU Ke-wei. Improving the crack resistance and fracture toughness of Cu/Ru multilayer thin films via tailoring the individual layer thickness [J]. Journal of Alloys and Compounds, 2018, 742: 45−53.

基于非均匀层片结构调控的累积叠轧铝合金层状金属复合材料力学性能优化

莫太骞[1,2]，肖华强[2]，尹存宏[2]，林 波[2]，王雪健[2]，马 凯[3]

1. 贵州大学 教育部现代制造技术重点实验室，贵阳 550025；
2. 贵州大学 机械工程学院，贵阳 550025；
3. 中国科学院 金属研究所 师昌绪先进材料创新中心，沈阳 110016

摘 要：采用累积叠轧(ARB)、冷轧和退火处理制备了具有非均匀层片结构的 1060/7050 Al/Al 层状金属复合材料，并结合微观结构表征、力学性能测试和原位断口形貌观察，研究了其强化机理。结果表明，在不同次数的 ARB 循环后，Al/Al 层状复合材料组成层之间存在明显微观结构差异。与轧制压下量分别为 37.5%和 50.0%的轧制态 2560 层 Al/Al 层状复合材料相比，轧制压下量为 62.5%的样品由于其在界面上相对较高的机械不相容性，退火处理后能够更有效地改善力学性能。在拉伸变形过程中，随着具有非均匀层片结构的 2560 层 Al/Al 层状复合材料中不相容性程度的增加，几何必需位错的密度随之增加以适应较大的应变梯度，导致更为显著的背应力强化效应和力学性能的改善。

关键词：Al/Al 层状金属复合材料；非均匀层片结构；几何必需位错；背应力强化

(Edited by Bing YANG)